Intrinsic and scattering attenuation in Chedrang Fault and its vicinity – the rupture area of Great Assam earthquake of 12 June 1897 (M = 8.7)

Saurabh Baruah[1,]*, Devajit Hazarika[2], Aditya Kalita[1] and Sumana Goswami[1]

[1]Geoscience Division, CSIR, North-East Institute of Science and Technology (formerly Regional Research Laboratory), Jorhat 785 006, India
[2]Wadia Institute of Himalayan Geology, Dehradun 248 001, India

The attenuation of seismic waves is one of the basic physical parameters used in seismological studies, which is closely related to the seismicity and tectonic activity of a particular area. In the present study, attenuation properties of the crust beneath the Chedrang Fault and its vicinity, the rupture area of the great Assam earthquake of 12 June 1897 (M = 8.7) are studied using waveforms recorded by a local seismic network composed of five stations. In total 20 local earthquakes have been analysed to estimate (i) coda wave attenuation quality factor (Q_c) applying single scattering model, (ii) total attenuation quality factor (Q_d) from direct S-wave applying spectral ratio method and (iii) intrinsic and scattering attenuation quality factors (Q_i and Q_s) following the Wennerberg's approach. Coda Q (Q_c) values are obtained using different coda window lengths (20, 30 and 40 s) for frequency bands centred at 1, 1.5, 2, 3, 4, 6, 8, 12, 16 and 18 Hz. This study indicates that Q_c increases with increasing lapse time and that Q_c is frequency dependent following the attenuation–frequency relation $Q_{c(20)} = 36.29 \pm 1.18f^{1.45 \pm 0.09}$, $Q_{c(30)} = 69.92 \pm 1.11f^{1.23 \pm 0.06}$ and $Q_{c(40)} = 117.08 \pm 1.08f^{1.07 \pm 0.05}$ for 20, 30 and 40 s respectively. This behaviour is usually correlated to the presence of heterogeneity in the crust and to the degree of tectonic complexity underneath the study area. The Q_c^{-1} values for this area follow a substantially similar trend of Q_c^{-1} decay with frequency as the other tectonically active regions of the world.

Finally, from the separation of Q_s and Q_i values, it is observed that the study area can be characterized by a low scattering attenuation (small scattering Q inverse, Q_s^{-1}) and by a relatively high intrinsic attenuation (high intrinsic Q inverse, Q_i^{-1}).

Keywords: Chedrang Fault, coda waves, frequency dependence, intrinsic attenuation seismic waves, quality factor.

THE Chedrang Fault and its vicinity bounded by lat. 25°–26.4°N and long. 90°–91.8°E belongs to the western part of Shillong Plateau. It covers much of the maximum intensity (XII) zone of the great Assam earthquake of 12 June 1897 (ref. 1). This earthquake is a prominent among the great earthquakes of the world because of the large area over which it caused damage, liquefaction and landslides[2]. The earthquake almost totally destroyed settlements and small towns on the western part of the plateau and caused heavy damage in the surrounding areas mainly due to the extensive liquefaction to the ground. A relatively high level of microearthquake activity is still observed in the region[3–6].

Earthquake damage is primarily caused by seismic waves and shaking is heavily influenced by the manner in which seismic waves propagate through complex geological structures[7]. When seismic waves propagate through the earth, the wave amplitude decays with travel distance defining attenuation characteristics of the media. The knowledge of seismic wave attenuation in a given region is necessary to obtain information on earthquake source parameter and also for the assessment of seismic hazard in a region[8–10]. The attenuation of high frequency seismic wave is expressed as an inverse of quality factor Q (ref. 11), i.e. Q^{-1} and it is a useful tool to study the attenuation properties of the media towards understanding the physical laws related to seismic wave propagation. Seismic wave attenuation described by quality factor Q is a complex mechanism. The main contributing factors towards Q are intrinsic attenuation (Q_i^{-1}) due to medium anelasticity and scattering attenuation (Q_s^{-1}) associated with inhomogeneities. Quantitative contribution of these factors is important for correct geological and tectonic interpretation[7,12–21].

The main objective of this study is to obtain the attenuation properties of the crust beneath the Chedrang Valley area of the active Shillong Plateau by using local earthquakes and to ascertain the estimates of the quality factor of direct S-wave (Q_d) and coda wave (Q_c). Finally, the intrinsic attenuation (Q_i^{-1}) and scattering attenuation (Q_s^{-1}) are separated.

The coda wave attenuation quality factor, Q_c, is estimated applying single scattering model of Aki[22], modified by Aki and Chouet[23] and Sato[24]. In this method, coda

*For correspondence. (e-mail: saurabhb_23@yahoo.com)

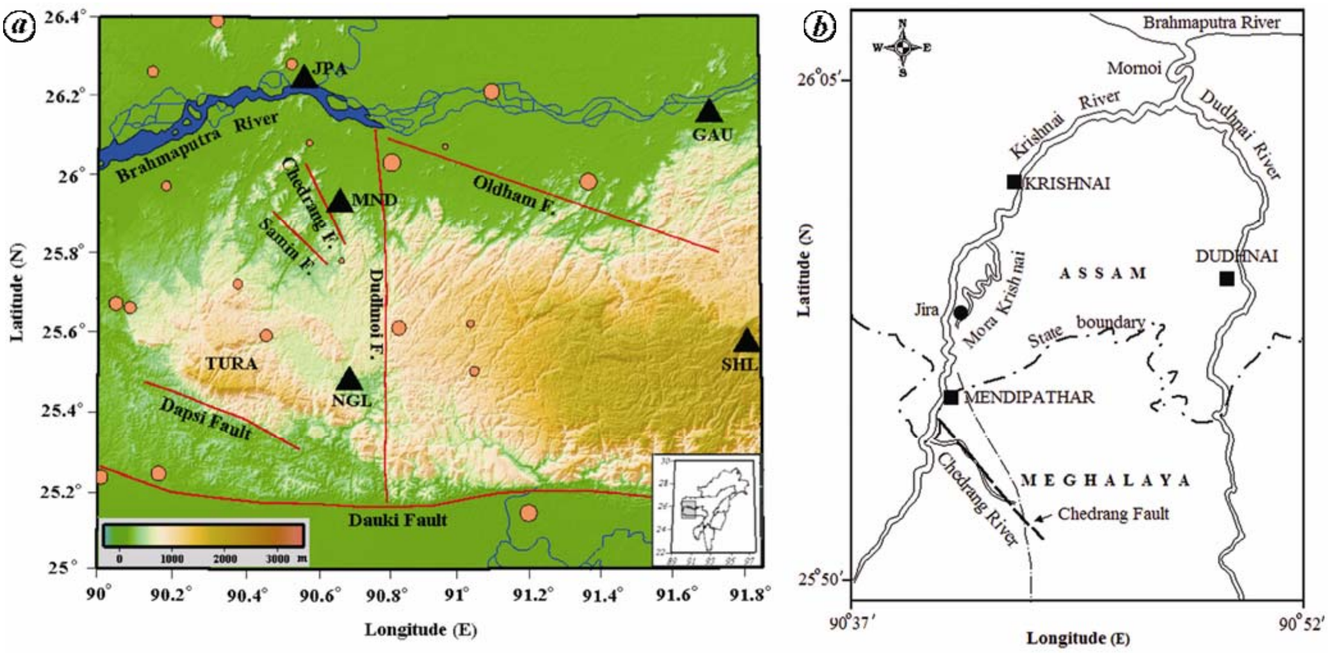

Figure 1. ***a***, Tectonic map of the study area with epicentral distribution of 20 events (filled circles) recorded at five stations (triangles) used for this analysis. ***b***, Close view of Chedrang Fault area with rivers and canals.

waves of local earthquakes are considered as backscattered S to S-waves[25] and are generated when S-wave encounters the different heterogeneities present in randomly but uniformly in the earth's crust. This method has been widely used because of its simplicity and ease of application to get estimates of local and regional Q_c (refs 10 and 26–32). Q_c has been extensively estimated in many regions of the world and it has proven to be an extremely sensitive parameter of the geological environment[33].

In order to estimate the total quality factor from direct S-wave (Q_d), the spectral ratio methods by Tsujiura, and Frankel[34] and Wennerberg[35] are used. These methods provide the most direct approach to measure the energy loss in a seismic signal.

In this study, the intrinsic (Q_i^{-1}) and scattering (Q_s^{-1}) attenuations are estimated using Q_c and Q_d values following Wennerberg[36] for Chedrang Valley and its vicinity in the north-eastern region. The results of this study are highlighted here.

Tectonic settings

Tectonically, Chedrang Valley and its vicinity (Figure 1 *a*) belong to a highly complex zone, which is a component of the western part of Shillong Plateau surrounded by Main Boundary Thrust (MBT) to the north and thick tertiary sediment cover to the south[37]. Geologically, Shillong Plateau has evolved during the Mesozoic to Tertiary times with an average elevation of about 1 km. Dauki Fault (DF) is a major fault in the region, where 1000 m south facing escarpment of Bengal basin exists. The northern side is bordered by the Brahmaputra Valley. The western side is characterized by an N–S trending Dhubri Fault (DhF), which separates Garo Hills (western Shillong Massif) from the Indian subcontinent that separates the ancient continental crust of the Indian Shield from the cretaceous ocean floor. Apart from these, tectonics of this region is influenced by several faults, viz. Chedrang, Dudhnoi, Samin and Dapsi faults oriented NW–SE, N–S, NW–SE and E–W respectively[1,37,38]. Chedrang Fault is oriented along Chedrang River and joins the Krishnai River, a tributary of the Brahmaputra river (Figure 1 *b*). The old course of the Krishnai River (presently called as 'Mora Krishnai' in local language i.e. dead Krishnai) prior to the 1897 earthquake lies towards western side of the present course[1]. At the offset zone of the Krishnai river, a village named 'Jira' was converted into a lake during the 1897 Great Assam Earthquake. The lake (the old course of river Krishnai) is 1.5 km away from the confluence of the Chedrang and Krishnai rivers. The upliftment took place along the eastern side of the Chedrang Fault passing through the village, resulting in the formation of the lake. The fault appears to be an expression of the fracture close to the Chedrang River. Oldham[1] observed an 11 m co-seismic slip down to the west of location of the Chedrang Fault. Formation of the lake near Jhira village is an indication of the slip. A recent palaeoseismic study[39] from fissures and sand blown structures in the region identifies northern boundary fault as a major seismic source, now termed as Brahmaputra Fault. Besides, Angelier and Baruah[40] tried to reconstruct the stress regimes with a stress analysis of focal mechanism

Table 1. Hypocentral parameters of the events used in the study

Date	Origin time h	min	s	Location Latitude (°N)	Longitude (°E)	Focal depth (km)	Magnitude (M_DA)
19-11-2001	12	16	43.43	26.03	90.82	27	3.8
25-11-2001	18	3	55.08	25.98	91.37	12	3.6
08-12-2001	22	8	57.99	26.21	91.10	12	3.4
12-12-2001	23	6	8.21	25.14	91.20	14	3.6
20-08-2003	19	28	22.20	25.50	91.05	11	1.8
20-08-2003	11	52	26.00	25.67	90.05	13	2.5
23-08-2003	00	57	47.20	25.61	90.84	14	2.7
23-08-2003	11	35	33.70	26.28	90.54	9	2.0
29-09-2003	21	15	27.41	25.62	91.04	21	1.5
30-09-2003	12	36	40.30	25.66	90.09	18	2.1
30-09-2003	18	14	18.24	25.24	90.17	24	2.7
01-10-2003	18	51	24.20	26.39	90.33	23	2.5
02-10-2003	17	37	38.29	25.97	90.19	8	1.8
03-10-2003	07	30	43.90	26.08	90.59	6	1.4
04-10-2003	03	48	24.29	25.72	90.39	15	1.8
04-10-2003	15	18	15.60	25.23	90.01	25	2.3
05-10-2003	21	02	55.00	25.78	90.68	17	1.4
08-10-2003	16	53	42.85	25.59	90.47	20	2.1
13-10-2003	11	19	33.36	26.26	90.15	16	2.0
19-10-2003	18	50	46.14	26.07	90.97	10	1.4

solutions of earthquakes to clarify the tectonic interaction and the underlying dynamics.

Data

We analysed 20 local earthquakes (Table 1) recorded during 2001 and 2003 by the local broadband seismic network. The network is operated by the North–East Institute of Science and Technology (formerly Regional Research Laboratory), Jorhat; National Geophysical Research Institute, Hyderabad (NGRI-Hyd) and Indian Meteorological Department, Shillong (IMD) (Figure 1 *a*). All the events are of the magnitude range 1.4–3.8 and are recorded in a epicentral distance of less than 100 km with shallow depth 6–27 km. The individual stations are equipped with Gurlap CMG-3ESP/CMG-3T sensors and high dynamic range 24 bit, REFTEK-72A series data acquisition system. All the stations are GPS time synchronized and the sampling rate is fixed at 100 samples per second. The parameters of the seismic stations (name, station code and location) are listed in Table 2. Only waveforms with high signal-to-noise ratio are selected eliminating clipped signals with electronic spikes. Before analysis, the seismograms are corrected for instrument response of respective recording stations. The hypocentral parameters, viz. origin time, latitude, longitude, focal depth and magnitude of the events have been computed using Hypocenter Location Program of Lienert *et al.*[41] with an average root mean square (rms) 0.03 s, epicentre and depth error < 1 km, based on the crustal velocity model of Mukhopadhyay *et al.*[42]. The epicentral locations of these events are shown in Figure 1.

Method and data analysis

Estimation of Q_c

Following Aki and Chouet[23] and Sato[24], the rms of coda wave amplitudes $A(f, t)$ in a seismogram for central frequency f over a narrow band width signal and lapse time, t measured from origin time of the earthquake can be expressed as:

$$A(f,t) = C(f)K(r,x)\exp(-\pi ft/Q_c), \tag{1}$$

where Q_c is the quality factor of coda wave, $C(f)$ takes into account the terms of source and site amplification and $K(r, x)$ is a function of station–source distance (r) and defined as:

$$K(r,x) = 1/r \cdot 1/x \cdot \ln[(x+1)/(x-1)], \tag{2}$$

where $t/t_s = x$ (t_s is the travel time of S-wave). Lapse time is taken to be the average time of beginning of a coda window as measured from the origin time plus half the window length, as specified in Gusev[43].

Taking natural logarithm of eq. (1) and rearranging the terms yields:

$$\ln[A(f,t)/K(r,x)] = \ln C(f) - \pi ft/Q_c. \tag{3}$$

For narrow bandpass filtered seismogram, $C(f)$ is constant. Therefore, from the slope of linear eq. (3) between $\ln[A(f, t)/K(r, x)]$ and t, the estimation of Q_c can be made as a function of frequency. The slope of the linear fit is $-\pi f/Q_c$.

Table 2. Parameters of seismological stations (e.g. name, code, their location and elevation) used for the present study

Station	Station code	Location: Latitude (°N)	Location: Longitude (°E)	Elevation (m)
Gauhati University	GAU	26.152	91.667	69
Jogighopa	JPA	26.239	90.575	42
Mendipather	MND	25.924	90.676	40
Nangalbibra	NGL	25.472	90.702	330
Shillong	SHL	25.566	91.859	1590

Table 3. Parameters of bandpass filter showing central frequencies with respective low and high cut-off frequencies

Low cut-off (Hz)	Central frequency (Hz)	High cut-off (Hz)
0.67	1.0	1.33
1.00	1.5	2.00
1.33	2.0	2.67
2.00	3.0	4.00
2.67	4.0	5.33
4.00	6.0	8.00
5.33	8.0	10.67
8.00	12.0	16.00
10.67	16.0	21.33
12.00	18.0	24.00

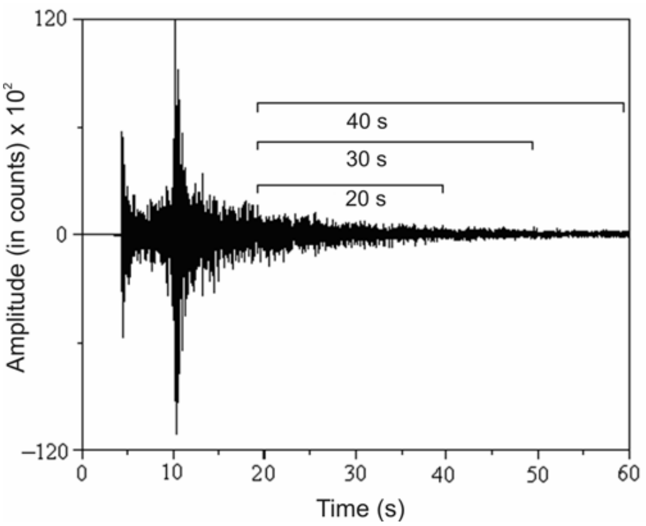

Figure 2. A vertical component seismogram recorded by MND–Mendipather Seismic Station. Selection of different coda window length is also shown.

For the estimation of Q_c values at different central frequencies (f_c), the seismograms are filtered using Butterworth bandpass filter of eight poles[44]. Ten frequency bands (bandwidth 0.67 f_c) are used for this purpose. The filter parameters are listed in Table 3. Coda window in each seismogram is considered after the time duration $2t_s$, where t_s is the travel time of direct S-wave[45]. An example showing different coda window length considered for analysis in a vertical component seismogram recorded by Mendipather (MND) Seismic Station is shown in Figure 2. The coda waves for all the filtered seismograms are smoothed calculating rms values of amplitudes of the filtered seismograms in a time window of 5.12 s for lower (1 and 1.5 Hz) and 2.56 s for higher (3–18 Hz) frequency bands with a sliding window along the coda in steps of half of the coda window length, i.e. 2.56 s and 1.28 s respectively. Once the set of $A(r, \omega, t)/K(r, x)$ and the coda intervals t are obtained, then using eq. (3) we can find out Q_c values from the slope of the linear fit.

Estimation of Q_d

Q_d is estimated using the spectral ratio method[34,35]. In this method, the spectral amplitude of a body wave $A(f)$ at frequency f is related to travel time t, source receiver distance r and quality factor Q_d by

$$A(f) \propto \left[\frac{A_0(f)R(f)\exp(-\pi ft/Q_d)}{r}\right], \quad (4)$$

where $A_0(f)$ is the spectral amplitudes at the source, $R(f)$ the response function of the site to the incoming seismic radiation. For amplitudes at two different frequencies f_1 and f_2, the natural logarithm of their amplitude ratio is given by:

$$\ln[A(f_1)/A(f_2)] = \ln[A_0(f_1)/A_0(f_2)] + \ln[R(f_1)/R(f_2)] - [\pi(f_1 - f_2)t/Q_d]. \quad (5)$$

If $A_0(f_1)/A_0(f_2)$ and $R(f_1)/R(f_2)$ are constant for all events under study and independent of travel time, then eq. (5) is a straight line with the slope $-\pi(f_1 - f_2)/Q_d$. From this slope, Q_d can easily be calculated with known values of f_1 and f_2.

Attenuation quality factor of direct S-wave (Q_d) is computed for all the events (Table 1) using the spectral ratio method[24,46]. In this study, f_1 is chosen at 1 Hz and f_2 = 1.5, 2, 3, 4, 6, 8, 12, 16 and 18 Hz respectively. The logarithm of spectral amplitude ratios, $[A(f_1)/A(f_2)]$ at different frequencies are plotted against travel time of

S-wave for all the events, the slope of which gives Q_d at each value of f_2.

Estimation of Q_i *and* Q_s

We have followed Wennerberg[36] for estimation of Q_i and Q_s from Q_c and Q_d estimates. The quality factor of direct S-wave (Q_d) estimated for an earth volume equivalent to volume sampled by coda wave can be considered as the total attenuation and can be related to Q_i and Q_s as[47]

$$\frac{1}{Q_d} = \frac{1}{Q_i} + \frac{1}{Q_s}. \tag{6}$$

In addition, Q_c^{-1} values can be expressed as a function of Q_i and Q_s by the relationship[36]

$$\frac{1}{Q_c} = \frac{1}{Q_i} + \frac{1-2\delta(\tau)}{Q_s}, \tag{7}$$

where $1 - 2\delta(\tau) = -1.00/(4.44 + 0.738\tau)$ and $\tau = \omega t/Q_s$, with $t(= t_c + W/2)$ the average lapse time and ω the angular frequency. Using eqs (6) and (7) as a system of equations, Q_s^{-1} and Q_i^{-1} can be expressed as

$$\frac{1}{Q_s} = \frac{1}{2\delta(\tau)}\left(\frac{1}{Q_d} - \frac{1}{Q_c(\tau)}\right), \tag{8}$$

$$\frac{1}{Q_i} = \frac{1}{2\delta(\tau)}\left(\frac{1}{Q_c(\tau)} + \frac{2\delta(\tau)-1}{Q_d}\right). \tag{9}$$

For estimation of Q_i and Q_s from these equations, it is necessary to compute Q_c and Q_d.

Q_i and Q_s are estimated from the corresponding values of Q_c and Q_d using eqs (6)–(9).

Results

Q_c values are estimated from the filtered coda waves of 75 waveforms of 20 local events in frequency bands centered at 1, 1.5, 2, 3, 4, 6, 8, 12, 16 and 18 Hz for different coda window lengths of 20, 30 and 40 s. First, the result obtained on Q_c estimation using 30 s window length has been discussed to portray the attenuation characteristics of the region and later the Q_c estimates using 20 and 40 s are discussed.

A total of 434 Q_c measurements are obtained for 30 s window lengths, which fulfil the criteria of having correlation coefficient 60%, estimated from linear regression of $\ln[A(f, t)/K(r, x)]$ versus t plot. The value of Q_c measurements varies from 10 to 85 at frequency 1 Hz and 1010 to 3600 at 18 Hz (Figure 3 *a*). This variation may be due to different focal depths of the events (6–27 km) and epicentral distance and local site specific geological conditions. The mean Q_c values vary from 58 ± 14 at 1 Hz to 2067 ± 350 at 18 Hz as shown in Figure 3 *b*, it is observed that Q_c values follow a power law of the form $Q_c = Q_0 f^n$, where Q_0 is the quality factor Q_c at 1 Hz and n the degree of frequency dependence[25]. For 30 s coda window, Q_0 and n are 69.92 ± 1.11 and 1.23 ± 0.058 respectively and follow attenuation relation $Q_c = 69.92 \pm 1.11 f^{1.23 \pm 0.058}$. This empirical attenuation relation provides average attenuation characteristics of the medium of a localized zone around the study area. According to Sato[24] and Pulli[27], the scatterers responsible for generation of coda waves can be assumed to be distributed over the surface area of an ellipsoid, which can be calculated using

$$\frac{X^2}{(vt/2)^2} + \frac{Y^2}{[(vt/2)^2 - R^2/4]} = 1, \tag{10}$$

where X and Y are the major and minor axes of the ellipsoid, and R the source–receiver distance for all the event–station pairs used. Since the station–source distance of the present data set is less (< 100 km), R may be ignored and then eq. (10) will represent circular area of radius $vt/2$. The parameter v represents the velocity of Lg wave (3.5 km/s), and t $(= t_c + W/2)$ the average lapse time. Here, t_c is the average starting time of the coda window, and W the coda window length. The maximum depth of volume of medium from which coda wave generation would occur for different lapse times is given by

$$h = \sqrt{[(vt/2)^2 - (R/2)^2]} + h_{av}, \tag{11}$$

where h_{av} is the average hypocentral depth. For average coda window length of 30 s and considering the velocity of 3.5 km/s, it is observed that coda wave samples a surface area of 2756.25 sq. km with a radius 52.5 km.

A comparison of Q_c^{-1} estimated at 30 s coda window as a function of frequency has been made in Figure 4 with Q_c^{-1} observations for other tectonically active regions of the world, e.g. Hindukush[26], Alaska[48], Garhwal Himalaya[49], Stone Canyon[23], Koyna India[8], northwest Himalaya[50], Chamoli region[31,43], etc. This figure shows that Q_c^{-1} values of the study area follow a trend substantially similar to those of the other tectonically active regions mentioned here and also with the theoretically predicted curve given by Sato[51].

The seismograms are analysed for Q_c estimation at 20–40 s lapse time window to study the effect of increasing coda window length on the estimation of Q_c values. For all these coda window lengths, Q_c values increase with increase in frequency. The value of Q_c estimated at 20, 30 and 40 s coda length has been averaged at each

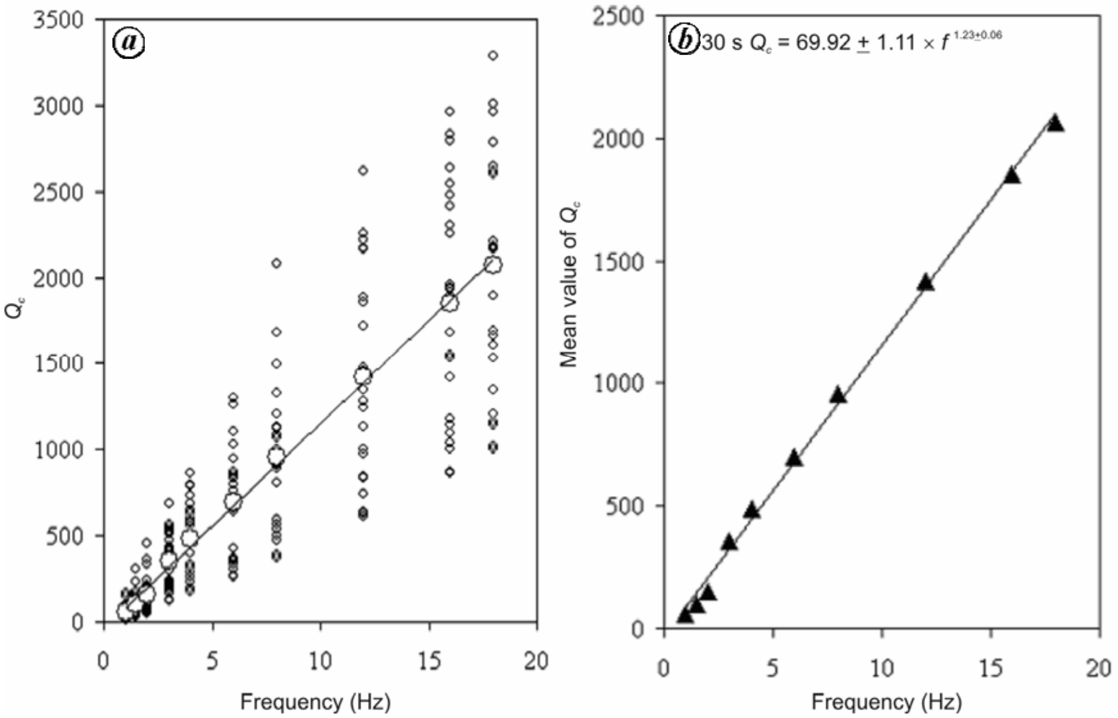

Figure 3. ***a***, Plot of all Q_c values as a function of frequency using 30 s coda window length. ***b***, Plot of mean values of Q_c as a function of frequency. A power law of the form $Q_c = Q_0 f^n$ has also been fitted using all mean values as shown.

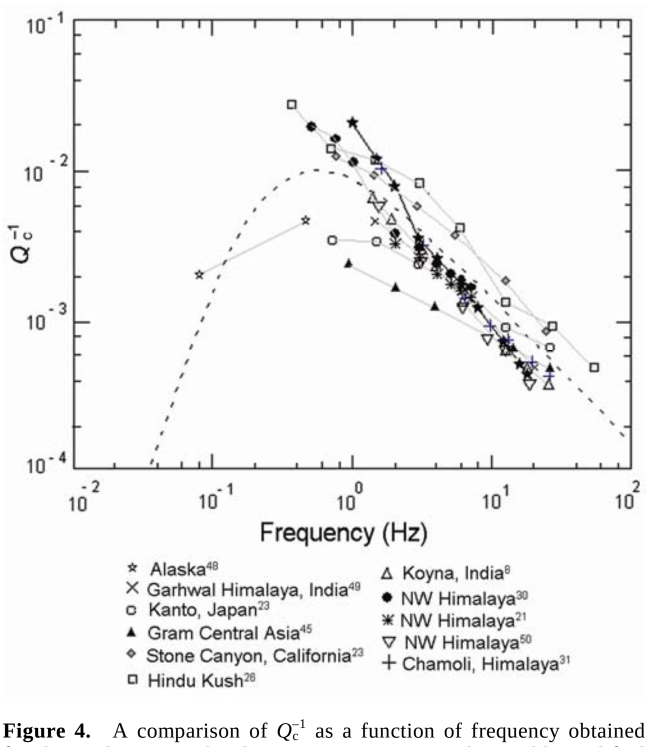

Figure 4. A comparison of Q_c^{-1} as a function of frequency obtained for the study area with other tectonic regions in the world (modified after Gupta *et al.*[8]).

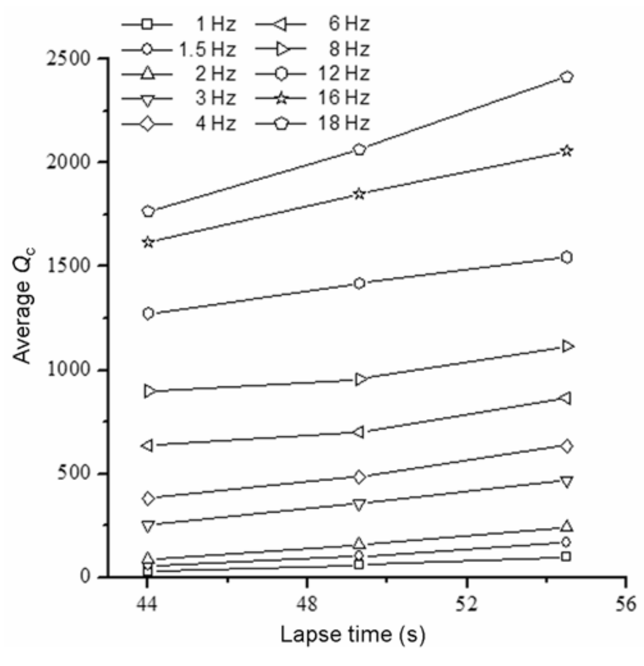

Figure 5. Variation of average Q_c estimated at each frequency with lapse time.

frequency. The variation of average Q_c values with lapse time in different frequencies is well reflected in Figure 5. The average Q_c values increase almost linearly with increase in lapse time with a little exception in 8 Hz. This may be due to less number of Q_c observations in that particular frequency. The average Q_c values estimated from 20, 30 and 40 s lapse time window length have been listed in Table 4. The mean value of Q_c as a function of frequency shows an increasing trend with the increasing lapse time window length (Figure 6). The mean value of Q_c for 20 s window varies from 28 ± 12 (at 1 Hz) to 1766 ± 209 (at 18 Hz) and for 40 s window Q_c varies from 99 ± 26 (at 1 Hz) to 2416 ± 402 (at 18 Hz). The empirical attenuation relations obtained for 20 and 40 s are $Q_c = 36.29 \pm 1.18 f^{1.45 \pm 0.09}$ and $Q_c = 117.08 \pm 1.08 f^{1.07 \pm 0.05}$ respectively.

Q_d is computed using the same data set used for estimation of Q_c. The Q_d values obtained at frequencies 1.5, 2, 3, 4, 6, 8, 12, 16 and 18 Hz have been averaged at each frequency. It is observed that the Q_d values increase with frequency following the frequency dependent average attenuation relationship $Q_d = 32.46 \pm 1.24 f^{1.50 \pm 0.11}$. The average Q_d varies with frequency as shown in Figure 7. Relatively the values of Q_d are observed to be less than Q_c. At higher frequencies (> 6 Hz) Q_d and Q_c become closer (Table 5).

Using the Wennerberg's[36] approach, Q_i and Q_s are separated from Q_d and Q_c estimates. The estimated Q_s varies from 74 at 1.5 Hz to 79,040 at 18 Hz following the power law $Q_s = 37.53 \pm 1.42 f^{2.68 \pm 0.18}$. Moreover the degree of frequency dependence ($n = 2.68$) suggests that attenuation due to scattering decreases rapidly with increase in frequency. The estimated Q_i varies from 82 at 1.5 Hz to 2049 at 18 Hz following the power law $Q_i = 62.21 \pm 1.16 f^{1.25 \pm 0.08}$. Comparing the value of degree of frequency dependence (n) for Q_i and Q_s with that for Q_c and Q_d, it is observed that, in higher frequencies the contribution of intrinsic attenuation towards the total attenuation is more compared to scattering attenuation in the region. This is clearly visible from the plot showing variation of Q_c^{-1}, Q_d^{-1}, Q_i^{-1}, Q_s^{-1} with frequency (Figure 8).

Table 4. Measures of average Q_c values for different coda window length and frequencies

	Coda window length		
Frequency (Hz)	20 s	30 s	40 s
1	28 ± 12	58 ± 14	99 ± 26
1.5	54 ± 14	100 ± 15	165 ± 27
2	85 ± 21	155 ± 27	240 ± 46
3	252 ± 26	355 ± 39	470 ± 59
4	382 ± 31	486 ± 65	636 ± 96
6	636 ± 73	700 ± 82	864 ± 101
8	900 ± 105	955 ± 113	1115 ± 127
12	1273 ± 149	1419 ± 201	1545 ± 223
16	1619 ± 168	1851 ± 321	2057 ± 338
18	1766 ± 209	2067 ± 350	2416 ± 402

Table 5. Values of Q_c (for 30 s coda window length), Q_d, Q_s and Q_i at different frequencies

Frequency (Hz)	Q_c	Q_d	Q_s	Q_i
1.5	100	39	74	82
2	155	81	206	133
3	355	243	986	322
4	486	315	1141	435
6	700	628	8012	681
8	955	899	20204	940
12	1419	1309	22214	1391
16	1851	1742	38978	1823
18	2067	1998	79040	2049

Discussion and conclusion

An estimate of seismic wave attenuation is made in the Chedrang Valley and its vicinity including separation of intrinsic and scattering attenuation. As a result of this

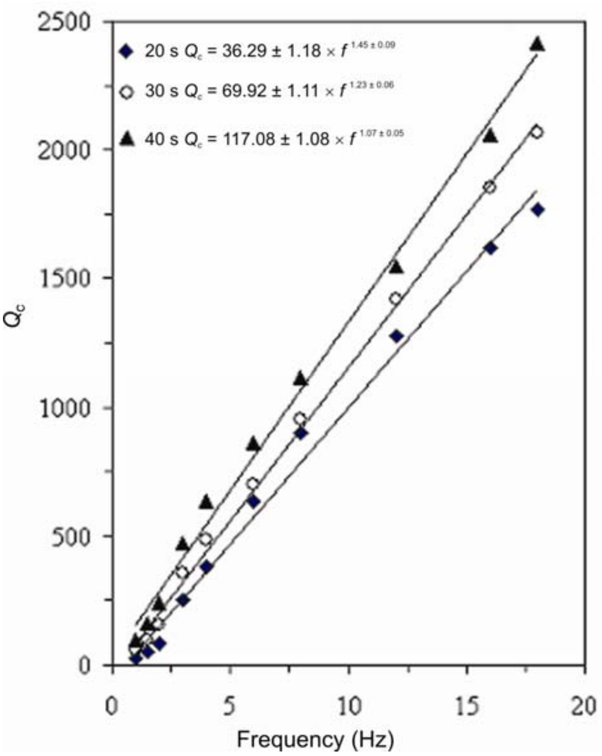

Figure 6. A comparison of mean values of Q_c as a function of frequency obtained at three lapse time windows. The power law fitted for each window is also shown.

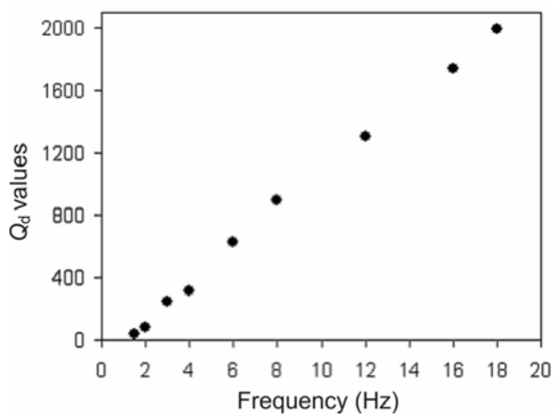

Figure 7. Plot of average Q_d values versus frequency.

separation, it is possible to recover a better comprehension of the physical mechanism governing attenuation properties of the crust of this region.

The single scattering model of Aki[22] modified by Aki and Chouet[23] and Sato[24] is applied to the data set consisting of 20 events to study Coda-Q(Q_c) and its frequency and lapse-time dependence. It is observed that average Q_c values are almost linearly frequency and lapse-time dependent. The lapse-time dependence is generally interpreted[26,52,53] as due to depth dependence of the seismic attenuation, which generally decreases with depth. The more the increase in lapse time, the larger the area of deeper crust that is sampled by the coda waves[30,31,54]. Therefore, increase in Q_c values with the increase of coda window length indicates that the deeper crust is less heterogeneous (high Q_c) than to the shallow crust (low Q_c).

The Q_c measurements in the study area exhibit a much stronger frequency dependence. Comparison of attenuation (Q_c^{-1}) measurement as a function of frequency for the region with Q_c^{-1} measurements observed for other tectonic regions of the world shows that Q_c^{-1} values of the region follow a substantially similar trend of Q_c^{-1} decay with frequency as the other tectonic regions and also a theoretically predicted curve by Sato[51]. The world data is obtained from various research publications. Variation of Q_0 and n in the attenuation relationship for different tectonic regions have been the subject of many studies and many investigators brought out a positive correlation between low Q_0 and the area of high tectonic activity[26,29,55]. Jin and Aki[56] interpreted that the regions with high tectonic activity are characterized by low Q_0 values. Several studies[26,53,55] also observed a strong correlation between n and the level of tectonic activity. Generally the regions having high n value are tectonically more active compared to regions with low n. For example, a stable region such as central United States has low n (n = 0.2, ref. 57), whereas in our study area $n > 1$. This observation is in conformity with the present microseismic activities in the study area.

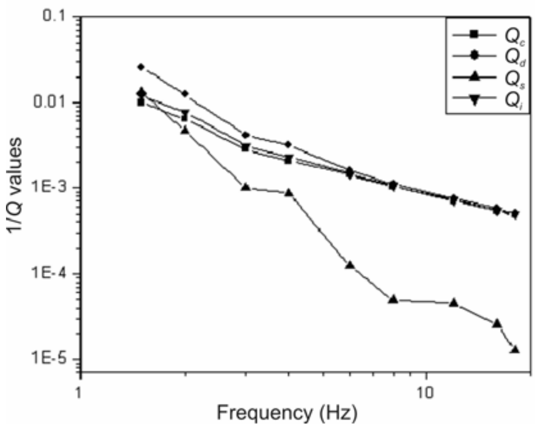

Figure 8. Plot showing variation of Q_c^{-1}, Q_d^{-1}, Q_s^{-1} and Q_i^{-1} with frequency.

The coda Q method proposed by Aki and Chouet[23] is a promising means to study seismic wave attenuation in the crust. One of the problems in this method is the ambiguity in interpreting Q_c^{-1} in terms of total attenuation (Q_d^{-1}), scattering attenuation (Q_s^{-1}) and intrinsic attenuation (Q_i^{-1}). Few studies[23,33,57] indicate that Q_c is a combination of Q_i and Q_s; whereas studies by Aki[25] and Tsujiura[34] indicate that scattering attenuation plays a more significant role than intrinsic attenuation in case of coda decay. On the other hand, Shang and Gao[58] proposed that in a highly scattered medium, coda decay is mainly caused by intrinsic attenuation. Some laboratory experiments[59] and theoretical studies[60,61] demonstrated that Q_c^{-1} is not a measure of total attenuation but mainly reflects intrinsic attenuation.

In the present study, the relative contribution of Q_s and Q_i towards Q_c and Q_d is observed. It is seen that at lower frequencies, Q_d values are less than the Q_c values (Table 5) and with increasing frequency, Q_c becomes closer to Q_d. This probably indicates that at higher frequency Aki's[25] assumption (that coda waves are essentially backscattered S-wave) holds true for the study area. At lower frequency (1.5 Hz) Q_s^{-1} is comparable to Q_i^{-1}, whereas with increasing frequency Q_i^{-1} becomes higher compared to Q_s^{-1}. Although all the Q parameters are frequency dependent with coefficients $n > 1$, the highest value of n corresponds to Q_s. Several authors[13,62–64] have suggested

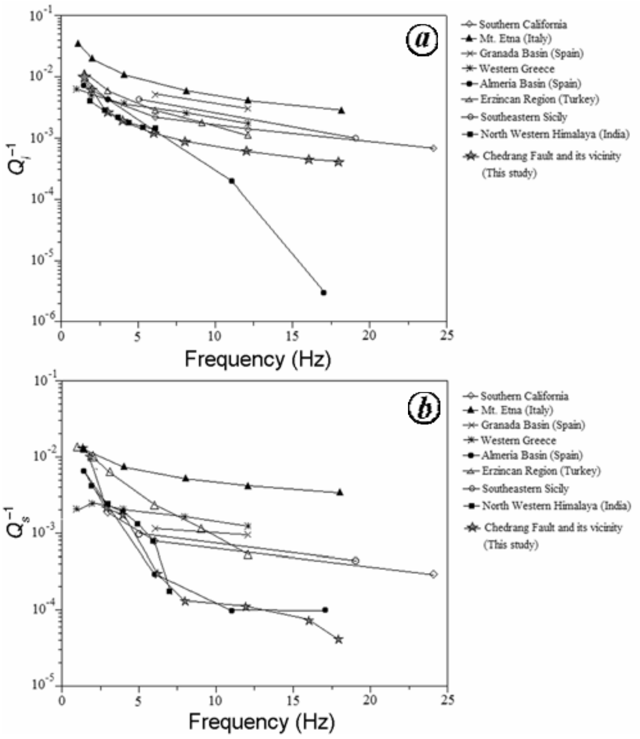

Figure 9. ***a***, Comparison of Q_i^{-1} and ***b***, Q_s^{-1} obtained for our study area with the observations observed for different regions: Southern California[68]; Mt Etna and Granada Basin[14]; Western Greece[69]; Almeria Basin[70]; Erzincan Region[71]; Southern Sicily[67]; North-Western Himalayas[20].

that this strong frequency dependence could be related to the size of heterogeneities. Frequency dependence of Q_s^{-1} occurs when the heterogeneity responsible for the scattering is comparable with wavelengths of the analysed lower frequency. This means that seismic scattering is related to fracture and lithological heterogeneity in the crust[65]. At higher frequency, predominance of intrinsic attenuation can be explained by thermal dissipation of heat in spatial domains at the microphysical scale as suggested by Leary[65]. The study area, i.e. Chedrang Fault and its vicinity is characterized by NNW–SSE compression with predominant thrust faulting[66] which may lead to development of microfracture and small cracks. This type of microfractures also induces thermal gradients of sufficient magnitudes to allow for the thermal absorption needed for the seismic wave absorption observation.

A comparison is made of Q_i^{-1} and Q_s^{-1} values for the study area with that of various parts of the world[20,67]. An useful comparison in Figure 9, where the pattern of intrinsic and scattering attenuation estimated throughout the world and the present study is reported. The pattern of Q_i^{-1} and Q_s^{-1} with frequency is analogous to the estimates obtained in other tectonic areas in the world, except with the observation that of Q_i^{-1} obtained in Spain. Comparing the value of degree of frequency dependence (n) for Q_i and Q_s, it is observed that, in higher frequencies the contribution of intrinsic attenuation towards the total attenuation is more compared to scattering attenuation in the Chedrang Valley and its vicinity.

1. Oldham, R. D., Report of the great earthquake of 12 June 1897. *Mem. Geol. Surv. India*, 1899, **29**, 1–379.
2. Ambraseys, N. and Bilham, R., Re-evaluated intensities for the great Assam earthquake of 12 June 1897, Shillong, India. *Bull. Seismol. Soc. Am.*, 2003, **93**, 655–673.
3. Khattri, K. N., Mukhopadhyay, S., Subrahmaniam, C. and Rao, A., Seismotectonic studies in the western part of the Shillong massif regions. In 8th Symposium on Earthquake Engineering, Roorkee, 29–31 December 1986, vol. 1, pp. 103–110.
4. Mukhopadhyay, S., Chander, R. and Khattri, K. N., Fine structure of seismotectonics in western Shillong massif, north east India. *Proc. Indian Acad. Sci.* (*Earth Planet. Sci.*), 1993, **102**, 383–398.
5. Kayal, J. R., Microseismicity and source mechanism study: Shillong Plateau, Northeast India. *Bull. Seismol. Soc. Am.*, 1987, **77**, 184–194.
6. Kayal, J. R. and De, R., Microseismicity and tectonics in Northeast India. *Bull. Seismol. Soc. Am.*, 1991, **81**, 131–138.
7. Tuve, T., Bianco, F., Ibanez, J., Patane, D., Del Pezzo, E. and Bottari, A., Attenuation study in the Straits of Messina area (southern Italy). *Tectonophysics*, 2006, **421**, 173–185.
8. Gupta, S. C., Teotia, S. S., Rai, S. S. and Gautam, N., Coda *Q* estimates in the Koyna Region, India. *Pure Appl. Geophys.*, 1998, **153**, 713–731.
9. Ugalde, A., Tripathi, J. N., Hoshiba, M. and Rastogi, B. K., Intrinsic and scattering attenuation in western India from aftershocks of the 26 January 2001 Kachchh earthquake. *Tectonophysics*, 2007, **429**, 111–123.
10. Biescas, B., Rivera Z. and Zapata, J. A., Seismic attenuation of coda waves in the eastern region of Cuba. *Tectonophysics*, 2007, **429**, 99–109.
11. Knopoff, L., *Q. Rev. Geophys.*, 1964, **2**, 625–660.
12. Hoshiba, M., Separation of scattering attenuation and intrinsic absorption in Japan using the multiple lapse time window analysis of full seismogram envelope. *J. Geophys. Res.*, 1993, **98**, 15809–15824.
13. Akinci, A., Del Pezzo, E. and Ibanez, J. M., Separation of scattering and intrinsic attenuation in southern Spain and western Anatolia (Turkey). *Geophys. J. Int.*, 1995, **121**, 337–353.
14. Del Pezzo, E., Ibanaz, J. M., Morales, J., Akinci, A. and Maresca, R., Measurements of intrinsic and scattering seismic attenuation in the crust. *Bull. Seismol. Soc. Am.*, 1995, **85**, 1373–1380.
15. Del Pezzo, E., Simni, M. and Ibanez, J. M., Separation of intrinsic and scattering *Q* for volcanic areas: a comparison between Etna and Campi Flegrei. *J. Volcanol. Geotherm. Res.*, 1996, **70**, 213–219.
16. Del Pezzo, E., Bianco, F. and Zaccarelli, L., Separation of Q_i and Q_s from passive data at Mt Vesuvius: a reappraisal of the seismic attenuation estimates. *Phys. Earth Planet. Int.*, 2006, **159**, 202–212.
17. Bianco, F., Castellano, M., Del Pezzo, E. and Ibanez, J. M., Attenuation of short-period seismic waves at Mt Vesuvius, Italy. *Geophys. J. Int.*, 1999, **138**, 67–76.
18. Bianco, F., Del Pezzo, E., Castellano, M., Ibanez, J. M. and Di Luccio, F., Separation of intrinsic and scattering seismic attenuation in the Southern Apennine zone, Italy. *Geophys. J. Int.*, 2002, **150**, 10–22.
19. Bianco, F., Del Pezzo, E., Malagnini, L., Di Luccio, F. and Akinci, A., Separation of depth-dependent intrinsic absorption and scattering seismic attenuation in the northeastern sector of the Italian peninsula. *Geophys. J. Int.*, 2005, **161**, 130–142.
20. Mukhopadhyay, S., Tyagi, C. and Rai, S. S., The attenuation mechanism of seismic waves in northwestern Himalayas. *Geophys. J. Int.*, 2006, **167**, 354–360.
21. Mukhopadhyay, S. and Tyagi, C., Variation of intrinsic and scattering attenuation with depth in NW Himalayas. *Geophys. J. Int.*, 2008, **172**, 1055–1065.
22. Aki, K., Analysis of the seismic coda of local earthquakes as scattered waves. *J. Geophys. Res.*, 1969, **74**, 615–631.
23. Aki, K. and Chouet, B., Origin of coda waves: source, attenuation, and scattering effects. *J. Geophys. Res.*, 1975, **80**, 3322–3342.
24. Sato, H., Energy propagation including scattering effects: single isotropic scattering. *J. Phys. Earth*, 1977, **25**, 27–41.
25. Aki, K., Attenuation of shear-waves in the lithosphere for frequencies from 0.05 to 25 Hz. *Phys. Earth Planet. Inter.*, 1980, **21**, 50–60.
26. Roecker, S. W., Tucker, B., King, J. and Hatzfeld, D., Estimates of *Q* in Central Asia as a function of frequency and depth using the coda of locally recorded earthquakes. *Bull. Seismol. Soc. Am.*, 1982, **72**, 129–149.
27. Pulli, J. J., Attenuation of coda waves in New England. *Bull. Seismol. Soc. Am.*, 1984, **74**, 1149–1166.
28. Reha, S., *Q* determined from local earthquakes in the south Carolina coastal plain. *Bull. Seismol. Soc. Am.*, 1984, **74**, 2257–2268.
29. Van Eck, T., Attenuation of coda wave in the dead sea region. *Bull. Seismol. Soc. Am.*, 1988, **78**, 770–779.
30. Mukhopadhyay, S. and Tyagi, C., The lapse time and frequency dependent attenuation characteristics of coda waves in North Western Himalayas. *J. Seismol.*, 2007, **11**, 149–158.
31. Mukhopadhyay, S., Sharma, J., Massey, R. and Kayal, J. R., Lapse time dependence of coda *Q* in the source region of the 1999 Chamoli earthquake. *Bull. Seismol. Soc. Am.*, 2008, **98**, 2080–2086.
32. Hazarika, D., Baruah, S. and Gogoi, N. K., Attenuation of coda waves in the Northeastern Region of India, *J. Seismol.*, 2009, **13**, 141–160.
33. Sato, H. and Fehler, M., *Seismic Wave Propagation and Scattering in the Heterogeneous Earth*, AIP Press, Springer Verlag, New York, 1998.

34. Tsujiura, M., Spectral analysis of coda waves from local earthquakes. *Bull. Earthquake Res. Inst*., 1978, **53**, 1–48.
35. Frankel, A. and Wennerberg, L., Microearthquakes spectra from the Anza, California, seismic network: site response and source scaling. *Bull. Seismol. Soc. Am.*, 1989, **79**, 581–609.
36. Wennerberg, L., Multiple-scattering interpretation of coda-*Q* measurements. *Bull. Seismol. Soc. Am.*, 1993, **83**, 279–290.
37. Nandy, D. R., *Geodynamics of Northeastern India and the Adjoining Region*, ABC Publications, Calcutta, 2001, p. 209.
38. Baruah, S. and Hazarika, D., A GIS based tectonic map of northeastern India. *Curr. Sci*., 2008, **95**, 176–177.
39. Rajendran, C. P., Rajendran, K., Duarah, B. P., Baruah, S. and Earnest, A., Interpreting the style of faulting and paleoseismicity associated with the 1897 Shillong, northeast India, earthquake: implications for regional tectonism. *Tectonics*, 2004, **23**, TC 4009.
40. Angelier, J. and Baruah, S., Seismotectonics in Northeast India: a stress analysis of focal mechanism solutions of earthquakes and its kinematic implications. *Geophys. J. Int*., 2009; doi:10.1111/j.1365-246X.2009.04107.x.
41. Lienert, B. R., Berg, B. E. and Frazer, L. N., Hypocenter: an earthquake location method using centered, scaled and adaptively damped least squares. *Bull. Seismol. Soc. Am*., 1986, **76**, 771–783.
42. Mukhopadhyay, S., Chander, R. and Khattri, K. N., Crustal properties in the epicentral tract of the Great 1897 Assam Earthquake, northeastern India. *Tectonophysics*, 1997, **283**, 311–330.
43. Gusev, A. A., Vertical profile of turbidity and coda. *Q*. *Geophys. J. Int*., 1995, **123**, 665–672.
44. Stearns, D. S. and David, R. A., *Signal Processing Algorithms*, Prentice-Hall, Inc., Englewood Cliffs, New Jersey, 1988.
45. Rautian, T. G. and Khalturin, V. I., The use of coda for determination of the earthquake source spectrum. *Bull. Seismol. Soc. Am*., 1978, **68**, 923–948.
46. Tsujiura, M., Frequency analysis of the seismic waves. *Bull. Earth. Res. Inst. Tokyo Univ*., 1966, **44**, 873–891.
47. Dainty, A. M., A scattering model to explain seismic *Q* observation in the lithosphere between 1 and 30 Hz. *Geophys. Res. Lett*., 1981, **8**, 1126–1128.
48. Aki, K., Source and scattering effects on the spectra of small local earthquakes. *Bull. Seismol. Soc. Am*., 1981, **71**, 1687–1700.
49. Gupta, S. C., Singh, V. N. and Kumar, A., Attenuation of coda waves in the Garhwal Himalaya, India. *Phys. Earth Planet. Int*., 1995, **87**, 247–253.
50. Kumar, N., Parvez, I. A. and Virk, H. S., Estimation of coda wave attenuation for NW Himalayan region using local earthquakes. *Phys. Earth Planet. Int.*, 2005, **151**, 243–258.
51. Sato, H., Attenuation of envelope formation of three-component seismograms of small local earthquakes in randomly inhomogeneous lithosphere. *J. Geophys. Res*., 1984, **89**, 1221–1241.
52. Ibanez, J. M., Del Pezzo, E., De Miguel, F., Herraiz, M., Alguacil, G. and Morales, J., Depth-dependent seismic attenuation in the Granada zone (Southern Spain). *Bull. Seismol. Soc. Am*., 1990, **80**, 1232–1244.
53. Akinci, A., Taktak, A. G. and Ergintav, S., Attenuation of coda waves in western Anatolia. *Phys. Earth Planet Inter*., 1994, **87**, 155–165.
54. Gupta, S. C. and Kumar, A., Seismic wave attenuation characteristics of three Indian regions: a comparative study. *Curr. Sci.*, 2002, **82**, 407–413.
55. Aki, K., Scattering and attenuation of shear waves in the lithosphere. *J. Geophys. Res.*, 1980, **85**, 6496–6504.
56. Jin, A. and Aki, K., Temporal change in coda *Q* before the Tangshen earthquake of 1976 and the Haicheng earthquake of 1975. *J. Geophys. Res*., 1986, **91**, 665–673.
57. Singh, S. K. and Herrmann, R. B., Regionalization of crustal coda *Q* in the continental United States. *J. Geophys. Res*., 1983, **88**, 527–538.
58. Shang, T. L. and Gao, L. S., Transportation theory of multiple scattering and its application to seismic coda waves of impulsive source. *Sci. Sin., Ser. B, Chem. Biol. Med. Earth Sci*., 1988, **31**, 1503–1514.
59. Matsunami, K., Laboratory tests of excitation and attenuation of coda waves using 2-D models of scattering media. *Phys. Earth Planet. Int*., 1991, **67**, 36–47.
60. Frankel, A. and Wennerberg, L., Energy-flux model of seismic coda: separation of scattering and intrinsic attenuation. *Bull. Seismol. Soc. Am*., 1987, **77**, 1223–1251.
61. Hoshiba, M., Simulation of multiple-scattered coda wave excitation based on the energy conservation law. *Phys. Earth. Planet. Int*., 1991, **67**, 123–136.
62. Mayeda, K., Koynagi, S., Hoshiba, M., Aki, K. and Zeng, Y., A comparative study of scattering, intrinsic and coda *Q* for Hawaii, Long Valley and Central California between 1.5 and 15 Hz. *J. Geophys. Res*., 1992, **97**, 6643–6659.
63. Canas, J. A., Ugalde, A., Pujades, L. G., Carracedo, J. C., Blonco, M. J. and Soler, V., Intrinsic and scattering seismic wave attenuation in the Canary Island. *J. Geophys. Res*., 1998, **103**, 15037–15049.
64. Giampiccolo, E., Tuve, T., Gresta, S. and Patane, D., S-waves attenuation and separation of scattering and intrinsic absorption of seismic energy in southern Sicily (Italy). *Geophys. J. Int*., 2006, **165**, 211–222.
65. Leary, P. C., Quantifying crustal fracture heterogeneity by seismic scattering. *Geophys. J. Int*., 1995, **122**, 125–142.
66. Baruah, S., Duarah, R. and Yadav, D. K., Pattern of seismicity in Shillong Mikir plateau and the orientation of principal compressive axis. *J. Geol. Soc. India*, 1997, **49**, 533–538.
67. Giampiccolo, E., Gresta, S. and Rascona, F., Intrinsic and scattering attenuation from observed seismic codas in Southeastern Sicily (Italy). *Phys. Earth. Planet. Int*., 2004, **145**, 55–66.
68. Jin, A., Mayeda, K., Adams, D. and Aki, K., Separation of intrinsic and scattering attenuation in southern California using TERRAscope data. *J. Geophys. Res*., 1986, **99**, 17835–17848.
69. Tselentis, G. A., Intrinsic and scattering seismic attenuation in W. Greece. *Pure Appl. Geophys*., 1998, **153**, 703–712.
70. Pujades, L. *et al*., Coda *Q* distribution in the Iberian Peninsula. *Geophys. J. Int*., 1991, **100**, 285–301.
71. Akinci, A. and Eydogan, H., Scattering and anelastic attenuation of seismic energy in the vicinity of north Anatolian fault zone, eastern Turkey. *Phys. Earth Planet. Inter*., 2000, **122**, 229–239.

ACKNOWLEDGEMENTS. We thank Dr P. G. Rao, Director, North–East Institute of Science and Technology, Jorhat for his constant encouragement and motivation and also for giving permission to publish the work. D.H. thanks to Dr B. R. Arora, Director, Wadia Institute of Himalayan Geology, Dehradun. We also thank the anonymous reviewer for his critical comment for encouragement which have improved the manuscript significantly.

Received 28 August 2009; revised accepted 15 July 2010